Front Matter

Title

Continuous monitoring of high-rise buildings using seismic interferometry

Authors

Aurélien Mordret[1*], Hao Sun[2], German A. Prieto[3], M. Nafi Toksöz[1], Oral Büyüköztürk[2]

Affiliations

[1] Department of Earth, Atmospheric and Planetary Sciences, Massachusetts Institute of Technology, Cambridge, Massachusetts, USA.
[2] Department of Civil & Environmental Engineering, Massachusetts Institute of Technology, Cambridge, Massachusetts, USA.
[3] Departamento de Geociencias, Universidad Nacional de Colombia - Sede Bogotá, Colombia.
[*] **Corresponding author:** Aurélien Mordret, Department of Earth, Atmospheric and Planetary Sciences, Massachusetts Institute of Technology, Cambridge, Massachusetts, USA. (mordret@mit.edu)

Abstract

The linear seismic response of a building is commonly extracted from ambient vibration measurements. Seismic deconvolution interferometry performed on ambient vibrations can be used to estimate the dynamic characteristics of a building, such as the shear-wave velocity and the damping. The continuous nature of the ambient vibrations allows us to measure these parameters repeatedly and to observe their temporal variations. We used 2 weeks of ambient vibration recorded by 36 accelerometers installed in the Green Building at the MIT campus to monitor the shear-wave speed and the apparent attenuation factor of the building. Due to the low strain of the ambient vibrations, we observe small speed changes followed by recoveries. We show that measuring the velocity variations for the deconvolution functions filtered around the fundamental mode frequency is equivalent to measuring the wandering of the fundamental frequency in the raw ambient vibration data. By comparing these results with local weather parameters, we show that the air humidity is the factor dominating the velocity variations in the Green Building, as well as the wandering of the fundamental mode. The one-day periodic variations are affected by both the temperature and the humidity. The apparent attenuation, measured as the exponential decay of the fundamental mode waveforms, is strongly biased by the amplitude of the raw vibrations and shows a more complex behavior with respect to the weather measurements. We have also detected normal mode non-linear interaction for the Green Building probably due to heterogeneity or anisotropy of its structure. We found that the temporal behavior of the frequency singlets may be used for monitoring.

Keywords: Building monitoring, ambient vibrations, deconvolution interferometry, relative seismic velocity changes, temporal variations, weather forcing, non-linearity.

Main text

Introduction

Seismic interferometry is a technique used to re-datum a source or sources recorded by two receivers to the location of one of the receiver and retrieve the wave propagation between the two receivers only (e.g., Schuster, 2009; Snieder et al., 2006; Wapenaar and Fokkema, 2006). Seismic interferometry has been applied in several fields of seismology to image the subsurface at different scales with surface waves (Lin et al., 2008; Mordret et al., 2014, 2015; Picozzi et al., 2009; Shapiro et al., 2005) or with body waves (Draganov et al., 2009; Wapenaar et al., 2008). When used with ambient vibrations (the so called seismic noise), seismic interferometry allowed seismologists to continuously monitor geological targets. Indeed, ambient vibrations can be recorded virtually continuously and everywhere on Earth, therefore, a repetitive utilization of seismic interferometry can be performed to follow the variations in time of the seismic wave propagation between pairs of receivers. This monitoring method has been originally developed to monitor volcano pre-eruptive behavior (Anggono et al., 2012; Brenguier et al., 2008b; Mordret et al., 2010; Sens-Schönfelder and Wegler, 2006) and crustal effects of large earthquakes (Brenguier et al., 2008a, 2014; Froment et al., 2013; Minato et al., 2012; Wegler et al., 2009).

In civil engineering applications, seismic interferometry was first introduced as NIOM method by Kawakami and Haddadi (1998); Kawakami and Oyunchimeg (2003) and later generalized by Snieder and Şafak (2006) to compute the time-domain impulse response function of the Millikan Library in Pasadena, California. The technique has become very popular since then (e.g., Ebrahimian et al., 2014; Kohler et al., 2007; Rahmani et al., 2015; Todorovska, 2009; Todorovska and Trifunac, 2008a,b). The aforementioned studies use earthquake records as input excitation to determine the dynamic characteristics of the buildings. Due to the random and isolated occurrence of earthquakes, these signals are not well suited for continuous monitoring of civil structures (Nakata et al., 2013). The use of ambient vibrations, on the other hand, is more appropriate. Ambient vibrations can be recorded anywhere and at any time and have been used for building monitoring purpose through the measurement of the wandering of the modal frequencies (e.g., Clinton et al., 2006; Ditommaso et al., 2010; Mikael et al., 2013; Nayeri et al., 2008). These studies showed that this parameter is very sensitive to irreversible changes in the building structure, like defects and cracks caused by earthquakes. It is also sensitive to reversible variations like ambient temperature or humidity changes.

Prieto et al. (2010) showed that seismic interferometry could also be applied to ambient vibrations to retrieve the impulse response of a building. More recently, Nakata and Snieder (2014) used seismic interferometry on ambient vibration data to develop a continuous monitoring technique. Their time resolution of four days and the arrival picking technique they used were not appropriate to draw any conclusion about the potential causes of the observed shear-wave velocity variations inside the building. In this paper, we extend the idea proposed by Prieto et al. (2010) and Nakata et al. (2015) to show that with a finer temporal resolution of 6 hours and with more accurate seismic velocity variation tracking techniques, we are able to finely measure the relative velocity variations inside the Green Building (Massachusetts Institute of Technology campus, Cambridge, MA), as well as its apparent-attenuation variations. These temporal changes are then correlated with different local weather parameters like the temperature and humidity to infer which one affects the most the building.

Data and Methods

We used 15 days of data (between May 12 and May 27 , 2015) continuously recorded on 36 accelerometer channels deployed inside the Green Building.

The Green Building, currently the tallest building in Cambridge, was designed by I.M. Pei and constructed during the period of 1962–1964. It has an elevation of 83.7 m with a footprint of 16.5 m by 34 m. Mechanical rooms are located on the top two floors (i.e., 19th and 20th floors). Heavy meteorological and radio equipments are asymmetrically mounted on the roof (Fig. 1(b)). Three elevator shafts are located on the eastern side of the building (Fig. 1(c)) and two stairwells are placed symmetrically at the NE and NW corners of the building. The building is constructed of cast-in-place reinforced concrete. The eastern and western facades are composed of 25 cm thick shear walls running the height of the building. The thickness of floor slabs is typically 10 cm. The basement floor has a depth of 3.8 m below the grade. Taciroglu et al. (2016) showed that the building's dynamic behavior can be modeled by a simple shear beam. More detailed descriptions of the building characteristics can be found Çelebi et al. (2014); Taciroglu et al. (2016) and Sun et al. (2017), in which the sensor information and deployment are also given. The sensor array was designed for monitoring the NS and EW translational vibration, the torsion, and the base rocking motion. The sensor locations and orientations are shown in Fig 1a. Note that the sensors are installed below the floor slabs. Fig 1c illustrates the sensor locations at a typical floor. Because of these locations, the acceleration in each direction (u_0 for EW direction, v_0 for NS direction and θ_0 for torsional direction) needs to be decoupled and is computed using the following equations:

$$u_1 = u_0 - \theta_0 y_1 \quad (1)$$

$$v_1 = v_0 + \theta_0 x_1 \quad (2)$$

$$v_2 = v_0 + \theta_0 x_2 \,, \quad (3)$$

where u_1 is the measured acceleration along the EW direction, v_1 and v_2 are the measured accelerations along the NS direction close to the eastern and western shear walls respectively, x_1, x_2 and y_1 are the sensor coordinates in the $x - O - y$ coordinate system with $O = (0, 0)$ shown in Fig 1c (see Table I in Sun et al. (2017) for the numerical values of the station coordinates). Therefore, the decoupled accelerations are:

$$\theta_0 = \frac{v_1 - v_2}{x_1 - x_2} \quad (4)$$

$$u_0 = u_1 + \theta_0 y_1 \quad (5)$$

$$v_0 = \frac{x_2 v_1 - x_1 v_2}{x_2 - x_1} \,. \quad (6)$$

Figure 2 shows the spectrogram of the decoupled NS acceleration recorded on the roof of the Green building. The fundamental mode is observed as a constant spectral peak at 0.75 Hz, the first overtone at ∼2.55 Hz, the second overtone at 5 Hz (Çelebi et al., 2014) and the third overtone around 6.6 Hz. Obvious is the daily pattern of the man-made ambient noise with higher amplitudes during working hours and smaller amplitudes during the nights. The two weekends are also well observed (May 16-17 and May 23-25, with Memorial Day) with smaller noise amplitudes.

Pre-processing and Impulse response functions from deconvolution interferometry

Before combining the data from the different sensors and applying deconvolution interferometry, the records from individual channels are pre-processed to mitigate potential biases introduced by the non-stationarity of the recorded ambient vibrations. The raw data are high-pass filtered at 0.05 Hz, then, the amplitudes larger than 3 standard deviations of the 2 week-long record are replaced by the 3 standard deviation threshold value. Then, the two-week long records are chopped into 20 min long segments with 50% overlap and deconvolution interferometry is applied to each detrended segment such as:

$$D_{U_n}(z, z_0, t) = \mathcal{F}^{-1}\left(\frac{U_n(z,\omega)U_n^*(z_0,\omega)}{|U_n(z_0,\omega)|^2 + \alpha\langle|U_n(z_0,\omega)|^2\rangle}\right) , \tag{7}$$

where $D_{U_n}(z, z_0, t)$ is the deconvolution function for vibration type U (U being the Fourier transform of either θ_0, u_0 or v_0) between floors at elevations z_0 and z, in which n is the index of the 20 min segment (n = 1 .. 2159 in this study) and t the lag time. In the right-hand side of equation 7, $\mathcal{F}^{-1}$ is the inverse Fourier transform, ω is the angular frequency, $*$ is the complex conjugate, $\langle|U_n|^2\rangle$ the average power spectrum of U_n, and α = 0.5% is a regularization parameter stabilizing the deconvolution (Nakata and Snieder, 2014). An estimation of the building response function $D_U(z, z_0, t)$ is given by the average of the deconvolution functions over the two weeks:

$$D_U(z, z_0, t) = \frac{1}{N}\sum_{n=1}^{N} D_{U_n}(z, z_0, t)\,. \tag{8}$$

We tested different pre-processing parameters, with an amplitude threshold of 1.5 standard deviations instead of 3, a high-pass filtering at 0.1 Hz instead of 0.05 Hz and $\alpha = 10\%$ in equation 7. We observed that the different pre-processing approach affected only marginally our results, both for the velocity variation measurements and for the damping variation measurements. Figure 3 shows the central part of the estimated Impulse Response Functions (IRFs) for the north-south translational modes (Fig. 3a-d), the east-west translational modes (Fig. 3b-e) and the torsional modes (Fig. 3c-f), both in the time domain and in the frequency domain, for each floor, with a source at the ground level. We can clearly observe a wave pulse traveling up and down in the building, with varying speeds, depending on the type of vibration (the dashed-lines are for reference only, assuming a constant speed of $\sim$365 m/s, $\sim$320 m/s and $\sim$600 m/s for the NS translational modes, EW translational modes and torsional modes, respectively). These pulses result from the superposition of all normal modes of the building and their frequency spectra are discrete. At longer times only the resonance of the fundamental modes is visible because the fundamental mode attenuates more slowly (Snieder and Şafak, 2006, Fig. 4). We observe a clear symmetry between the negative and positive time-lags of the IRFs, both in phase and amplitude. While the phase symmetry is expected from the seismic interferometry theory, it should not be the case for the amplitudes because the attenuation always follows causality. The amplitudes should therefore increase with increasing negative time-lags (Snieder, 2007). The presence of ambient vibration sources inside the building may play the role of volumetric sources and balance the amplitudes at negative time-lags (Snieder, 2007).

Another way to measure the speed of the traveling waves inside the building is by looking at the deconvolution functions between the roof and the other floors, with the source on the roof. In this configuration, Rahmani and Todorovska (2013); Snieder and Şafak (2006) showed that the deconvolution functions are the superposition of an acausal up-going wave with a causal down-going wave. The speed of these waves is the shear wave speed of the building (Fig. 5). We note a discrepancy between the velocity of the NS modes measured with the source on the ground floor and the source on the roof. This could be due to dispersion or reflections caused by the internal structure of the building (Rahmani and Todorovska, 2013; Snieder and Şafak, 2006). In this framework, the IRF is not a superposition of modes but a broadband pulse having a continuous frequency spectrum. According to the shear-beam model of (Rahmani and Todorovska, 2013; Snieder and Şafak, 2006) the up- and down-going pulses vanish at ground level and are not sensitive to the soil-structure interaction. Moreover, the wavelength of the waves (on the order of 100 m) is much larger than the typical floor height so the scattering inside the building should be minimal. However, at low frequency, we observe potential internal reflections in the EW direction (Fig. 5b)). At higher frequency, a clear coda is following the main pulse and may be the consequence of multiple reflections at the base and inside the building (Fig. 5d) Rahmani and Todorovska, 2013).

Velocity-variation measurements

For monitoring applications the absolute value of the velocity does not need to be evaluated: only the relative velocity variations are needed. It is then possible to use techniques which are much more accurate that picking the absolute travel-times of seismic pulses propagating inside the building. The basic principle to measure relative seismic velocity variations (dv/v) is to compare a current waveform with a reference one by measuring their relative phase-shifts along the lag-time. Here, the current waveforms are the individual D_{U_n} waveforms averaged in a 6 hours moving window (average of the nth deconvolution function with the 35 previous ones) and the reference one is D_U. We used two common techniques to measure dv/v within the Green building: the Moving Window Cross-Spectral (MWCS) technique (Clarke et al., 2011), which is performed in the frequency domain and the stretching technique (Hadziioannou et al., 2009; Sens-Schönfelder and Wegler, 2006), which is performed in the time domain. The comparison of the results from both independent methods allows us to assess the accuracy and consistency of our measurements (Mordret et al., 2016).

The IRFs deconvolved by the ground floor present two distinct types of vibration: the propagating part at short lag times (-3 s $\lesssim t \lesssim$ 3 s), where the fundamental mode and the overtones are superposed, and the resonant part at large lag times (-25 s $\lesssim t \lesssim$ -6 s and 6 s $\lesssim t \lesssim$ 25 s), where the fundamental mode dominates. We chose to analyze separately these two kinds of vibration. The MWCS technique is performed within the previously described time windows using small sliding windows with a length 6 times the central period of interest. The small windows move by 0.1 s. For each small window, the cross-spectrum between the current and the reference waveform is computed. From this cross-spectrum, the coherence and the phase between the two signal as a function of the frequency is extracted. A weighted linear regression (weighted by the coherency) is performed on the phase in the frequency band of interest to extract the phase delay between the reference and current correlation, as well as an error estimate of the slope. Thus, for each small sliding window we obtain 3 values: a time delay (*tdelay*, in s), an error for the time delay (*errtdelay*, in s) and the average coherency between the two signals (*coh*). Then, these measurements are used in a second step to evaluate the relative velocity variation $dv/v = -dt/t$ between the reference and the current waveform. A weighted linear regression on the time delays with respect to the central time of the windows is used to calculate the final dv/v value and its uncertainty for a specific frequency band. Only the time delays with errors $errtdelay < 0.03$ s and coherency $coh > 0.8$ are used in the final linear regression to estimate dv/v. The uncertainty on the linear regression is taken as the uncertainties of the relative velocity variations.

The stretching technique (ST) is based on the assumption that if a small velocity change occurs homogeneously in the medium, then the current waveform will simply be a stretched or compressed version of the reference waveform. The stretching coefficient is therefore the relative velocity variation dv/v. Prior to the stretching measurement, the reference and current waveforms are filtered in the frequency band of interest. The measurement is performed using a grid search on the stretching coefficients. We sampled 300 stretching coefficients linearly spaced between -5% and 5%. For each coefficient, the time axis of the current waveform is stretched and then the current waveform is interpolated onto this new time axis. The correlation coefficient between the window of the stretched current waveform and the reference waveform is then computed and stored. The best dv/v measurement is chosen as the stretching coefficient that maximizes the correlation coefficient between the current stretched and reference waveforms. To refine the estimation of dv/v we use the maximum correlation coefficient and its nearest left and right neighbors. We perform a quadratic interpolation of these three points and take the stretching coefficient corresponding to the maximum of the interpolated curve. The error estimate is obtained from the expression derived by Weaver et al. (2011). The error is related to the maximum correlation coefficient, the size and the position of the window in the coda, the frequency bandwidth and the inverse of the central frequency of the signal. We notice that in our context, the errors measured by the MWCS technique are most of the time larger than the errors from the stretching technique. In the following, we only present the uncertainties are resulting from the MWCS technique to keep conservative values.

Damping measurements

The damping ratio of each mode can be computed by measuring the slope μ_i of the envelope of the IRFs band-pass filtered within the half-power bandwidth (Prieto et al., 2010; Snieder and Şafak, 2006; Sun et al., 2017). The damping ratio ξ_r is given by

$$\xi_r = \frac{1}{N_0 \omega_r} \sum_{i=1}^{N_0} |\mu_i| \, , \tag{9}$$

where N_0 is the number of observations (typically the number of instrumented floors) and ω_r is the rth resonant frequency. Nakata and Snieder (2014) showed that with ambient vibration deconvolution interferometry, when noise sources are inside the building, the damping ratio measured by the amplitude decay of the deconvolution function is a combination of the intrinsic damping of the building and the radiation loss in the solid Earth at the base of the building. Here, we measure the damping separately on the acausal and causal sides of the IRFs and our final estimation of the damping is the average of both sides.

Results

Figure 6 shows the 2159 IRFs (smoothed by a 6 hours moving window) for the NS translational mode, measured on the roof with a source at the ground level. We can directly observe a temporal variation of the overall amplitudes of the IRFs as well as time shifts of the phases within the later parts of the waveforms. The phase shifts will be analysed through the velocity variation measurements whereas the amplitude variations will be interpreted as damping variations and/or ambient noise sources variations.

Velocity variations

We measured the velocity variations in different lag-time windows along the waveforms and several frequency bands to assess the contribution of the propagation part from the resonant part and the contribution of the fundamental mode alone from the superposition of the overtones. In the following, we mainly analyze the NS translational modes, which have the higher signal-to-noise ratio and focus on records deconvolved either from the ground floor or from the roof. The two methods (MWCS and ST) are also compared in the aforementioned contexts.

Figure 7a) shows an example of dv/v measured in the central part of the IRFs (-3 s $< t <$ 3 s) at each instrumented floor, for records deconvolved by the ground floor. The velocity variations are similar at each floor. This is certainly because the Green building has not suffered strong damages, but one might expect this to change if damages are present. If this is the case, records at each floor can be used to invert for the variations of the floor stiffnesses (Sun et al., 2017) and therefore, a high density seismic network is absolutely necessary to localize a damage. On the other hand, in a low seismic risk area where buildings are less likely to be strongly damaged, the similarity between the dv/v at all floors shows that the number of sensors in a seismic array (to monitor the long term ageing of the structure for example) can be drastically reduced.

Figure 8a) and b) show a comparison of the dv/v measurements performed with the MWCS and ST methods for the central part (-3 s $< t <$ 3 s) and the later parts (15 s $< |t| <$ 24.5 s) of the IRFs, respectively. The two methods behave similarly in both cases, however, the dv/v signals differ depending on the analyzed time lags. The central part presents larger dv/v variations ($\pm$ 1%) with a noticeable daily periodicity and uncertainties on the order of 0.5%. The later part of the waveforms exhibits smaller dv/v fluctuations ($\pm$ 0.5%) and the daily periodicity is weaker; the uncertainties fluctuate around 0.25% in average. Certain periods present a strong scattering of the dv/v measurements in the late part measurements which correspond to departures of the ST measurements from the MWCS measurement in the central part. These periods correspond to times when the apparent damping is the strongest (Fig. 9) and, therefore, where the signal to noise ratio is the poorest in the coda. From these observations we can see that the ST is more sensitive to local ambient vibrations amplitudes variations than the MWCS technique. We also observe a longer term $\sim$8 days period on both measurements. The dv/v measurements performed on IRFs obtained by deconvolving by the roof (see Figure 5) instead of the ground floor exhibit similar features (Figure 10). For these IRFs, we take the central part as (-1 s $< t <$ 1 s) and the coda parts as (0.5 s $< |t| <$ 3 s). The IRFs computed with the virtual source on the roof are less sensitive to the ground coupling (Petrovic and Parolai, 2016; Rahmani and Todorovska, 2013; Snieder et al., 2006; Taciroglu et al., 2016) therefore, the strong similarity between velocity variation measurements carried from the roof virtual source IRFs and ground floor virtual source IRFs (Figure 10) shows that the observed variations are, at a first order, due to changes within the building. Moreover, according to the model of Rahmani and Todorovska (2013); Snieder et al. (2006), the broadband pulses generated by the roof deconvolution should vanish due to a null reflection coefficient at the ground level. We observe in the case of the Green Building that although small, the reflection coefficient is non-zero (and may be negative) and a clear coda exists after the main pulse. The nature of the waves in this coda is not clear in the context of ambient vibration interferometry with internal sources of vibration. In the case of earthquake interferometry however, Rahmani and Todorovska (2013) showed that the coda is made by the superposition of internal reflections and reflections at the base of the building (Figure. 5d)). The coda carries the same velocity variation information as the direct waves (Figure 10).

Apparent damping variations

Figure 9a) shows the time-series of the damping variations measured at each instrumented floor. Again, the curves are extremely similar at each floor, presenting a local minimum almost every day during morning hours and a maximum during the afternoon. This correlates strongly with the amplitudes of the raw ambient vibrations (Figure 9b)) and might indicate that the measured attenuation is biased and may only be apparent. Given equation 7, it is expected that some amplitude information of the raw records is kept in the deconvolution functions. The non-propagating ambient vibrations from sources inside the building are not corrected for by the deconvolution of the ground floor records. However, the apparent damping presents a clear non-linear relationship (Guéguen et al., 2016) with respect to the ambient vibration amplitude (Figure 9c)): above a certain level of vibration,the apparent damping seems to stabilize around 5.5 %.

As shown by Nakata and Snieder (2014), in theory the amplitude decay of the waveforms depends on both intrinsic attenuation of the building and ground coupling and cannot be easily separated. The observed apparent damping variations are therefore difficult to relate to a simple cause and difficult to interpret. In our case, when the amplitudes of the ambient vibrations are too small, the amplitude of the deconvolution functions are strongly biased by the amplitudes of the deconvolved waveforms and the damping measurements are unreliable. Above a certain level, however, when the SNR is high enough, the damping measurements seems to converge toward a constant value. We hypothesize that at low amplitude, the non-propagating noise dominates the raw signal and the amplitude information of the IRFs is not reliable whereas when the amplitudes are larger, the propagating vibrations are larger than the noise and the IRFs amplitude information is more reliable. Because of this apparent non-linearity, the correlation with weather parameters is difficult to estimate. The temperature, recorded on top of the Green Building shows a slight link with the apparent damping (the two curve are anti-correlated at $\sim$ 55 %, Figure 11a-b). We also observe a $\sim$ 6 hours delay between the air humidity variations and the damping variations but these estimations should be taken cautiously. There is no significant correlation with the temperature (Figure 11c-d).

Discussion

Link with the modal frequency wandering

Tracking the wandering of the fundamental mode frequency is a well-known technique to monitor the temporal variations of the stiffness of a building (e.g. Clinton et al., 2006; Mikael et al., 2013; Nayeri et al., 2008). Here, we show that monitoring the velocity variations of the up-going IRFs filtered around the fundamental mode frequency is equivalent to measure the wandering of the fundamental mode frequency. For a simple 1D oscillator, the relative variation of frequency

f, $\Delta f/f$ is given by Haney et al. (2015):

$$\frac{\Delta f}{f} = \frac{\Delta v}{v} - \frac{\Delta l}{l} \quad (10)$$

where v is the shear-wave velocity of the building and l its length. If we assume that the length of the building does not change, we find that the relative frequency variations are equal to the relative velocity variations. In the ideal shear-beam case, the equality between velocity and frequency variations is also true for their absolute variations (Çelebi et al., 2016). This is clearly illustrated by Figure 12 where we see that the relative velocity variations, independently on the measurement technique, follow closely the wandering of the NS fundamental translational mode frequency. This interferometry-based technique is not limited to the fundamental modes but can be applied to overtones as long as their frequency can be easily isolated in the IRFs. In our example, we chose the simplest method to measure the frequency wandering, i.e. tracking the maximum of the fundamental resonance peak in the spectrogram shown in Fig. 2, between 0.5 and 1 Hz (Clinton et al., 2006). This technique is limited by the size of the signal sample used to compute the amplitude spectrum which gives a finite frequency resolution. Other more robust techniques, providing higher frequency resolution exist, such as the Random Decrement Technique (e.g., Mikael et al., 2013), but it was not necessary to use them here to illustrate our example. In any case, dv/v measurements from interferometry are as robust as modal frequency wandering observations and can provide independent information about the continuous dynamic behavior of a building.

Influence of local weather parameters

The main goal of structural health monitoring is to detect (and locate) any structural damage affecting a building through measurement of its dynamic behavior (Sohn, 2007). The main assumption behind this concept is that any damage will modify the stiffness and/or energy dissipation of the building. Therefore, monitoring parameters sensitive to stiffness or attenuation, such as shear wave velocity and damping of the normal modes of a building should allow us to detect such damage. By comparing the dynamic response of the building between an 'intact state' and a 'damaged state', we should be able to assess the extent of the damage and take action in a safety perspective. However, defining what an 'intact state' is quite difficult because any structure responds to environmental forcing by reversibly changing its dynamic parameters. In order to detect damages as early as possible, we must be able to detect small damages and therefore we must correct our dynamic parameters measurements for these changes which are not associated with damages.

Here we show that the interferometric approach can be used to monitor continuously (and potentially in real-time) the 'intact state' dynamics of a building and the effects environmental parameters, such as temperature and air humidity, can have on its shear-wave speed propagation. Figure 13 shows the comparison and correlation between relative velocity measurements and air temperature and humidity time series. We display dv/v measured on the central part of the down-going IRFs and up-going IRFs for the temperature and humidity, respectively, but measurements on the later parts of the IRFs show similar results. We show only the positive time-lag of the cross-correlation between the dv/v and weather data because we are only interested in the causal actions of the weather onto the building. We observe a stronger correlation between dv/v and humidity than between dv/v and temperature. The humidity correlation is dominated by the longer period trend whereas the temperature exhibits a stronger daily period correlation. It seems that the temperature is negatively correlated with the velocity variations but we cannot rule out a positive correlation with a 12 hours delay. On the other hand, the positive correlation between the dv/v and the humidity is more robust and it seems that there is a 1 day delay between them. Time series longer than two weeks could help to determine the correlations between the parameters with more accuracy. It is also possible that the relationship between the weather forcing and the velocity variations depends on the actual forcing period (the daily forcing having a different linear relationship from the weekly forcing). It might also be a non-linear relationship, which would explain the small correlation coefficient between the temperature and the dv/v measurements.

As stated by Mikael et al. (2013), the temperature effect on high-rise building does not have a clear trend and may depend on the building itself. Some studies observe a positive correlation between stiffness and temperature (e.g. Clinton et al., 2006; Mikael et al., 2013; Yuen and Kuok, 2010) whereas others observe a negative correlation (Mikael et al., 2013; Xia et al., 2012) or even a mixed behavior (Mikael et al., 2013). In the case of the Green Building, the anti-correlation in phase is clear but the correlation in amplitude seems less robust. It can be noted, as observed by Simon and Strong (1968) that the direct solar heating on the southern face of the building has a strong influence compared to air temperature variations. We are lacking data of the amount of sunshine during the studied period to be able to corroborate these observations.

The humidity influence on modal frequencies has been less studied and most observations focused on the effects of heavy rainfalls. Clinton et al. (2006) report an increase of the fundamental mode frequency of the soil-structure system of the Millikan library after heavy rainfalls. This has been confirmed with modeling experiments by Todorovska and Al Rjoub (2006, 2009). However, they do not provide a comparison with the actual local air humidity. Results from Mikael et al. (2013), looking at rainfalls, are inconclusive by lack of strong events. The variations observed at the Green Building are unlikely caused by heavy rainfalls: only a small shower ($\sim$ 10 mm) occurred on May 19 around 12PM and was not followed by clear effects. Herak and Herak (2010) observed a high positive correlation between air humidity and frequency changes over a 19 months period, however, it is not clear if the correlation still holds on the daily or weekly period. In most cases, the humidity effect on vibrational behavior of a building is interpreted to be caused by changes in the soil-structure coupling more than by changes in the structure itself. The fact that we observe a strong correlation between the dv/v measured on the down-going IRFs, which are supposedly not sensitive to the ground coupling, and the humidity might indicate that the wetting of the concrete plays a significant role in the observed stiffness changes. Because of its age, the structural concrete of the Green Building (directly exposed to the weather conditions) most likely exhibits an increased porosity which in turn enhances its gas and water permeability by several order of magnitude compared to un-cracked concrete (e.g., Wang et al., 1997). The diffusion rate of moisture in cracked concrete can reach several centimeters per hour (Kanematsu et al., 2009; Wang et al., 1997), enough to penetrate the entire thickness of the shear walls of the Green Building. The moisturizing of the grain contacts induces a weakening of the concrete (e.g., Murphy et al., 1984; Pimienta et al., 2014) that leads to a reduction of the shear-wave speed.

Can non-linear mode interaction be used as a new monitoring tool?

A close inspection of the spectrogram presented in Figure 2 shows that the resonance peak around 6.6 Hz is actually made of, at least, three peaks. They are clearly observed on the blow-up in Figure 14a). Modal analysis applied on the up-going IRFs (Sun et al., 2017) shows that these frequencies correspond to the 4th NS translational mode: considering either the three frequencies altogether or separately, we observe the same mode shapes (Fig. 14b). This result is in contradiction with the work of Trocha (2013), reported by Taciroglu et al. (2016), who found the 3rd NS translational mode at 8.25 Hz. This phenomenon is not visible on the EW spectrograms, ruling out an imperfection in our horizontal components decoupling procedure.

Regardless the exact nature of this mode, we observe a clear wandering of these frequencies. This wandering has a similar temporal fluctuation profile than the wandering of the fundamental mode and the first overtone. It also exhibits the same relative variations with respect to the mean frequency (Fig. 15). The three frequency peaks present a parallel temporal behavior which could suggest a bilinear behavior of the 4th NS translational mode. A Single-Degree-Of-Freedom bilinear system is characterized by two frequencies f_1 and f_3 which correspond to two different states of the system (with two different stiffnesses, for example). These frequencies interact to give rise to a third frequency f_2 called bilinear frequency (Chu and Shen, 1992):

$$f_2 = \frac{2f_1f_3}{f_1 + f_3}\,. \tag{11}$$

Such behavior can be caused by the coupling of one translational mode with a torsional mode of nearby frequency (Boroschek and Mahin, 1991). In the case of the Green building, however, modeling suggests that there is no torsional mode around 6.5 Hz. Bilinearity can also be observed in beams with breathing cracks where the two states of the system correspond to the open crack and the closed crack (e.g. Bovsunovsky and Surace, 2015; Chondros et al., 2001; Chu and Shen, 1992; Yan et al., 2013, and references therein). This model could suggest the presence of ageing or fatigue cracks in the building. The fact that the splitting only affects the 4th translational mode would indicate that the cause of the bilinearity is well localized along the height of the building, potentially where floor drift is the largest.

Nonetheless, Figure 15 shows that the two strongest singlets (Mode 4_1 = f_1 and Mode 4_3 = f_3) behave similarly to Mode 1 and Mode 2 but seem to lack their daily periodicity. Interestingly, the difference between f_1 and f_3 shows a stronger daily periodicity while still retaining a similar fluctuation behavior as Mode 1 and Mode 2. This can be seen in Figure 16 where the cross-correlation between the weather parameters and both the Mode 4 wandering and the $f_3 - f_1$ fluctuations show results similar to dv/v measurements. The temporal variations of the non-linear behavior of Mode 4 could give new valuable informations about temporal changes of some asymmetries or heterogeneities of the Green Building. Given the high frequency of the 4th mode, this non-linear interaction would be sensitive, on first approximation, to heterogeneities on the order of the wavelength ($\sim$ 50 m in this study). If confirmed, the study of high frequency modes non-linear interaction would not only be useful for damage detection but also as a first step in damage localization due to their localized sensitivity. We believe that the first observations presented in this paper can stimulate future studies in this direction.

Conclusion

We show with this study that deconvolution interferometry performed on continuous ambient vibrations can be used to monitor the structural dynamics of a building during 'normal conditions' by computing empirical IRFs. By deconvolving the vibrations recorded inside the building either by the records at the ground floor or the records on the roof, we are able to repetitively measure the speed of the up- or down-going shear waves traveling inside the building and to track their temporal variations. The study of the exponential decay of the IRFs waveforms give access to the temporal changes of the building (and ground coupling) apparent damping which is strongly biased by the amplitudes of the raw records. Our data processing and the velocity monitoring techniques used, fairly simple to implement, allows us to obtain a temporal resolution of 6 hours and an accuracy on the order of 0.1 to 0.5 %.

We show that measuring the seismic velocity variations on IRFs filtered around a specific mode frequency is equivalent to measure the actual relative wandering of this modal frequency, a technique widely used to monitor buildings. Therefore, with the deconvolution interferometry technique we provide an independent and potentially complementary way to perform building monitoring. We compared our dv/v results with weather parameters and found a strong positive correlation with air humidity and a possible negative correlation with temperature. Longer time records would be necessary to clarify these relationships. Deconvolution interferometry can then be used as a powerful tool to study buildings dynamics under normal conditions. A better understanding of these natural and reversible variations would allow us to correct for them to be able to better detect structural damages.

Finally, we speculate that the fourth NS translational mode of the Green Building is split due to non-linear interaction in its structure. The temporal variations of the singlet difference seem to correlate with our dv/v and frequency wandering observations as well as with the weather data. If this observable is confirmed, we believe that it could provide a new tool to efficiently monitor building and potentially help to locate damages.

Data and Resources

Seismograms used in this study were collected as part of an USGS experiment. Data can be obtained from Dr. Mehmet Çelebi (celebi@usgs.gov), last accessed 30 May 2015.

Acknowledgments

The authors thank Nori Nakata and Maria Todorovska for their constructive reviews which helped to improve the quality of the paper. We also thank USGS for instrumenting the building and MIT for granting permission for the instrumentation. Scott Wade, building manager provided access to the building. Jim Smith and Jason De Cristofaro of USGS successfully installed the monitoring system. We finally thank Dr. Mehmet Çelebi for operating the instrumentation and for providing us with the data. The authors would like to acknowledge the support by the Royal Dutch Shell through the MIT Energy Initiative. A.M. and G.A.P. acknowledge support from NSF grant EAR-1415907.

References

Anggono, T., Nishimura, T., Sato, H., Ueda, H., and Ukawa, M. (2012). Spatio-temporal changes in seismic velocity associated with the 2000 activity of Miyakejima volcano as inferred from cross-correlation analyses of ambient noise. *Journal of Volcanology and Geothermal Research*, 247:93–107.

Boroschek, R. L. and Mahin, S. A. (1991). *Investigation of the seismic response of a lightly damped torsionally coupled building*. PhD thesis, University of California, Berkeley California, Earthquake Engineering Research Center Report 91/18.

Bovsunovsky, A. and Surace, C. (2015). Non-linearities in the vibrations of elastic structures with a closing crack: a state of the art review. *Mechanical Systems and Signal Processing*, 62:129–148.

Brenguier, F., Campillo, M., Hadziioannou, C., Shapiro, N., Nadeau, R., and Larose, E. (2008a). Postseismic relaxation along the San Andreas fault at Parkfield from continuous seismological observations. *Science*, 321(5895):1478–1481.

Brenguier, F., Campillo, M., Takeda, T., Aoki, Y., Shapiro, N., Briand, X., Emoto, K., and Miyake, H. (2014). Mapping pressurized volcanic fluids from induced crustal seismic velocity drops. *Science*, 345(6192):80–82.

Brenguier, F., Shapiro, N., Campillo, M., Ferrazzini, V., Duputel, Z., Coutant, O., and Nercessian, A. (2008b). Towards forecasting volcanic eruptions using seismic noise. *Nature Geoscience*, 1(2):126–130.

Çelebi, M., Toksöz, N., and Büyüköztürk, O. (2014). Rocking Behavior of an Instrumented

Unique Building on the MIT Campus Identified from Ambient Shaking Data. *Earthquake Spectra*, 30(2):705–720.

Çelebi, M., Ulusoy, H. S., and Nakata, N. (2016). Responses of a Tall Building in Los Angeles, California, as Inferred from Local and Distant Earthquakes. *Earthquake Spectra*, 32(3):1821–1843.

Chondros, T., Dimarogonas, A. D., and Yao, J. (2001). Vibration of a beam with a breathing crack. *Journal of Sound and vibration*, 239(1):57–67.

Chu, Y. and Shen, M.-H. (1992). Analysis of forced bilinear oscillators and the application to cracked beam dynamics. *AIAA journal*, 30(10):2512–2519.

Clarke, D., Zaccarelli, L., Shapiro, N., and Brenguier, F. (2011). Assessment of resolution and accuracy of the Moving Window Cross Spectral technique for monitoring crustal temporal variations using ambient seismic noise. *Geophysical Journal International*, 186(2):867–882.

Clinton, J. F., Bradford, S. C., Heaton, T. H., and Favela, J. (2006). The observed wander of the natural frequencies in a structure. *Bulletin of the Seismological Society of America*, 96(1):237–257.

Ditommaso, R., Parolai, S., Mucciarelli, M., Eggert, S., Sobiesiak, M., and Zschau, J. (2010). Monitoring the response and the back-radiated energy of a building subjected to ambient vibration and impulsive action: the Falkenhof Tower (Potsdam, Germany). *Bulletin of Earthquake Engineering*, 8(3):705–722.

Draganov, D., Campman, X., Thorbecke, J., Verdel, A., and Wapenaar, K. (2009). Reflection images from ambient seismic noise. *Geophysics*, 74(5):A63–A67.

Ebrahimian, M., Rahmani, M., and Todorovska, M. I. (2014). Nonparametric estimation of wave dispersion in high-rise buildings by seismic interferometry. *Earthquake Engineering & Structural Dynamics*, 43(15):2361–2375.

Froment, B., Campillo, M., Chen, J., and Liu, Q. (2013). Deformation at depth associated with the 12 May 2008 MW 7.9 Wenchuan earthquake from seismic ambient noise monitoring. *Geophysical Research Letters*, 40(1):78–82.

Guéguen, P., Johnson, P., and Roux, P. (2016). Nonlinear dynamics induced in a structure by seismic and environmental loading. *The Journal of the Acoustical Society of America*, 140(1):582–590.

Hadziioannou, C., Larose, E., Coutant, O., Roux, P., and Campillo, M. (2009). Stability of monitoring weak changes in multiply scattering media with ambient noise correlation: Laboratory experiments. *The Journal of the Acoustical Society of America*, 125(6):3688–3695.

Haney, M., Hotovec-Ellis, A., Bennington, N., De Angelis, S., and Thurber, C. (2015). Tracking changes in volcanic systems with seismic interferometry. *Encyclopedia of Earthquake Engineering*, pages 1–23.

Herak, M. and Herak, D. (2010). Continuous monitoring of dynamic parameters of the dgfsm building (zagreb, croatia). *Bulletin of Earthquake Engineering*, 8(3):657–669.

Kanematsu, M., Maruyama, I., Noguchi, T., Iikura, H., and Tsuchiya, N. (2009). Quantification of water penetration into concrete through cracks by neutron radiography. *Nuclear Instruments and Methods in Physics Research Section A: Accelerators, Spectrometers, Detectors and Associated Equipment*, 605(1):154–158.

Kawakami, H. and Haddadi, H. R. (1998). Modeling wave propagation by using normalized input-output minimization (NIOM). *Soil Dynamics and Earthquake Engineering*, 17(2):117–126.

Kawakami, H. and Oyunchimeg, M. (2003). Normalized input–output minimization analysis of wave propagation in buildings. *Engineering Structures*, 25(11):1429–1442.

Kohler, M. D., Heaton, T. H., and Bradford, S. C. (2007). Propagating waves in the steel, moment-frame Factor Building recorded during earthquakes. *Bulletin of the Seismological Society of America*, 97(4):1334–1345.

Lin, F.-C., Moschetti, M. P., and Ritzwoller, M. H. (2008). Surface wave tomography of the western United States from ambient seismic noise: Rayleigh and Love wave phase velocity maps. *Geophysical Journal International*, 173(1):281–298.

Mikael, A., Gueguen, P., Bard, P.-Y., Roux, P., and Langlais, M. (2013). The Analysis of Long-Term Frequency and Damping Wandering in Buildings Using the Random Decrement Technique. *Bulletin of the Seismological Society of America*, 103(1):236–246.

Minato, S., Tsuji, T., Ohmi, S., and Matsuoka, T. (2012). Monitoring seismic velocity change caused by the 2011 Tohoku-oki earthquake using ambient noise records. *Geophysical Research Letters*, 39(9).

Mordret, A., Jolly, A., Duputel, Z., and Fournier, N. (2010). Monitoring of phreatic eruptions using interferometry on retrieved cross-correlation function from ambient seismic noise: Results from Mt. Ruapehu, New Zealand. *Journal of Volcanology and Geothermal Research*, 191(1):46–59.

Mordret, A., Landès, M., Shapiro, N., Singh, S., and Roux, P. (2014). Ambient noise surface wave tomography to determine the shallow shear velocity structure at Valhall: depth inversion with a Neighbourhood Algorithm. *Geophysical Journal International*, 198(3):1514–1525.

Mordret, A., Mikesell, D., Harig, C., Lipovsky, B. P., and Prieto, G. A. (2016). Monitoring south-west greenland's ice sheet melt with ambient seismic noise. *Science Advances*.

Mordret, A., Rivet, D., Landès, M., and Shapiro, N. M. (2015). Three-dimensional shear velocity anisotropic model of Piton de la Fournaise Volcano (La Réunion Island) from ambient seismic noise. *Journal of Geophysical Research: Solid Earth*, 120(1):406–427.

Murphy, W. F., Winkler, K. W., and Kleinberg, R. L. (1984). Frame modulus reduction in sedimentary rocks: the effect of adsorption on grain contacts. *Geophysical Research Letters*, 11(9):805–808.

Nakata, N. and Snieder, R. (2014). Monitoring a Building Using Deconvolution Interferometry. II: Ambient-Vibration Analysis. *Bulletin of the Seismological Society of America*, 104(1):204–213.

Nakata, N., Snieder, R., Kuroda, S., Ito, S., Aizawa, T., and Kunimi, T. (2013). Monitoring a Building Using Deconvolution Interferometry. I: Earthquake-Data Analysis. *Bulletin of the Seismological Society of America*, 103(3):1662–1678.

Nakata, N., Tanaka, W., and Oda, Y. (2015). Damage Detection of a Building Caused by the 2011 Tohoku-Oki Earthquake with Seismic Interferometry. *Bulletin of the Seismological Society of America*.

Nayeri, R. D., Masri, S. F., Ghanem, R. G., and Nigbor, R. L. (2008). A novel approach for the structural identification and monitoring of a full-scale 17-story building based on ambient vibration measurements. *Smart Materials and Structures*, 17(2):025006.

Petrovic, B. and Parolai, S. (2016). Joint Deconvolution of Building and Downhole Strong-Motion Recordings: Evidence for the Seismic Wavefield Being Radiated Back into the Shallow Geological Layers. *Bulletin of the Seismological Society of America*, 106(4):1720–1732.

Picozzi, M., Parolai, S., Bindi, D., and Strollo, A. (2009). Characterization of shallow geology by high-frequency seismic noise tomography. *Geophysical Journal International*, 176(1):164–174.

Pimienta, L., Fortin, J., and Guéguen, Y. (2014). Investigation of elastic weakening in limestone and sandstone samples from moisture adsorption. *Geophysical Journal International*, 199(1):335–347.

Prieto, G. A., Lawrence, J. F., Chung, A. I., and Kohler, M. D. (2010). Impulse response of civil structures from ambient noise analysis. *Bulletin of the Seismological Society of America*, 100(5A):2322–2328.

Rahmani, M., Ebrahimian, M., and Todorovska, M. I. (2015). Time-wave velocity analysis for early earthquake damage detection in buildings: application to a damaged full-scale RC building. *Earthquake Engineering & Structural Dynamics*, 44(4):619–636.

Rahmani, M. and Todorovska, M. I. (2013). 1D system identification of buildings during earthquakes by seismic interferometry with waveform inversion of impulse responsesmethod and application to Millikan library. *Soil Dynamics and Earthquake Engineering*, 47:157–174.

Schuster, G. T. (2009). *Seismic interferometry*, volume 1. Cambridge University Press Cambridge.

Sens-Schönfelder, C. and Wegler, U. (2006). Passive image interferometry and seasonal variations of seismic velocities at Merapi Volcano, Indonesia. *Geophysical research letters*, 33(21).

Shapiro, N. M., Campillo, M., Stehly, L., and Ritzwoller, M. H. (2005). High-resolution surface-wave tomography from ambient seismic noise. *Science*, 307(5715):1615–1618.

Simon, I. and Strong, P. (1968). Measurement of static and dynamic response of the Green Building at the MIT campus to insolation and wind. *Bulletin of the Seismological Society of America*, 58(5):1631–1638.

Snieder, R. (2007). Extracting the greens function of attenuating heterogeneous acoustic media from uncorrelated waves. *The Journal of the Acoustical Society of America*, 121(5):2637–2643.

Snieder, R. and Şafak, E. (2006). Extracting the building response using seismic interferometry: Theory and application to the Millikan Library in Pasadena, California. *Bulletin of the Seismological Society of America*, 96(2):586–598.

Snieder, R., Sheiman, J., and Calvert, R. (2006). Equivalence of the virtual-source method and wave-field deconvolution in seismic interferometry. *Physical Review E*, 73(6):066620.

Sohn, H. (2007). Effects of environmental and operational variability on structural health monitoring. *Philosophical Transactions of the Royal Society of London A: Mathematical, Physical and Engineering Sciences*, 365(1851):539–560.

Sun, H., Mordret, A., Prieto, G. A., Toksöz, M. N., and Büyüköztürk, O. (2017). Bayesian characterization of buildings using seismic interferometry on ambient vibrations. *Mechanical Systems and Signal Processing*, 85:468–486.

Taciroglu, E., Çelebi, M., Ghahari, S. F., and Abazarsa, F. (2016). An investigation of soil-structure interaction effects observed at the mit green building. *Earthquake Spectra*, 32(4):2425–2448.

Todorovska, M. I. (2009). Seismic interferometry of a soil-structure interaction model with coupled horizontal and rocking response. *Bulletin of the Seismological Society of America*, 99(2A):611–625.

Todorovska, M. I. and Al Rjoub, Y. (2006). Effects of rainfall on soil–structure system frequency: examples based on poroelasticity and a comparison with full-scale measurements. *Soil Dynamics and Earthquake Engineering*, 26(6):708–717.

Todorovska, M. I. and Al Rjoub, Y. (2009). Environmental effects on measured structural frequenciesmodel prediction of short-term shift during heavy rainfall and comparison with full-scale observations. *Structural Control and Health Monitoring*, 16(4):406–424.

Todorovska, M. I. and Trifunac, M. D. (2008a). Earthquake damage detection in the Imperial County Services Building III: analysis of wave travel times via impulse response functions. *Soil Dynamics and Earthquake Engineering*, 28(5):387–404.

Todorovska, M. I. and Trifunac, M. D. (2008b). Impulse response analysis of the Van Nuys 7-storey hotel during 11 earthquakes and earthquake damage detection. *Structural control & health monitoring*, 15(1):90.

Trocha, P. A. (2013). *Characterization of structural properties and dynamic behavior using distributed accelerometer networks and numerical modeling*. PhD thesis, Massachusetts Institute of Technology.

Wang, K., Jansen, D. C., Shah, S. P., and Karr, A. F. (1997). Permeability study of cracked concrete. *Cement and Concrete Research*, 27(3):381–393.

Wapenaar, K. and Fokkema, J. (2006). Greens function representations for seismic interferometry. *Geophysics*, 71(4):SI33–SI46.

Wapenaar, K., van der Neut, J., and Ruigrok, E. (2008). Passive seismic interferometry by multidimensional deconvolution. *Geophysics*, 73(6):A51–A56.

Weaver, R. L., Hadziioannou, C., Larose, E., and Campillo, M. (2011). On the precision of noise correlation interferometry. *Geophysical Journal International*, 185(3):1384–1392.

Wegler, U., Nakahara, H., Sens-Schönfelder, C., Korn, M., and Shiomi, K. (2009). Sudden drop of seismic velocity after the 2004 Mw 6.6 mid-Niigata earthquake, Japan, observed with passive image interferometry. *Journal of Geophysical Research: Solid Earth (1978–2012)*, 114(B6).

Xia, Y., Chen, B., Weng, S., Ni, Y.-Q., and Xu, Y.-L. (2012). Temperature effect on vibration properties of civil structures: a literature review and case studies. *Journal of civil structural health monitoring*, 2(1):29–46.

Yan, G., De Stefano, A., Matta, E., and Feng, R. (2013). A novel approach to detecting breathing-fatigue cracks based on dynamic characteristics. *Journal of Sound and Vibration*, 332(2):407–422.

Yuen, K.-V. and Kuok, S.-C. (2010). Ambient interference in long-term monitoring of buildings. *Engineering Structures*, 32(8):2379–2386.

Authors addresses

Aurélien Mordret, 77 Massachusetts Avenue, Department of Earth, Atmospheric and Planetary Sciences, Massachusetts Institute of Technology, Cambridge, Massachusetts, 02139-4307, USA. (mordret@mit.edu)

Hao Sun, 77 Massachusetts Avenue, Department of Civil & Environmental Engineering, Massachusetts Institute of Technology, Cambridge, Massachusetts, 02139-4307, USA. (haosun@mit.edu)

Germán A. Prieto, Departamento de Geociencias, Universidad Nacional de Colombia - Sede Bogotá, Colombia. (gaprietogo@unal.edu.co)

M. Nafi Toksöz, 77 Massachusetts Avenue, Department of Earth, Atmospheric and Planetary Sciences, Massachusetts Institute of Technology, Cambridge, Massachusetts, 02139-4307, USA. (toksoz@mit.edu)

Oral Büyüköztürk, 77 Massachusetts Avenue, Department of Civil & Environmental Engineering, Massachusetts Institute of Technology, Cambridge, Massachusetts, 02139-4307, USA. (obuyuk@mit.edu)

List of Figures

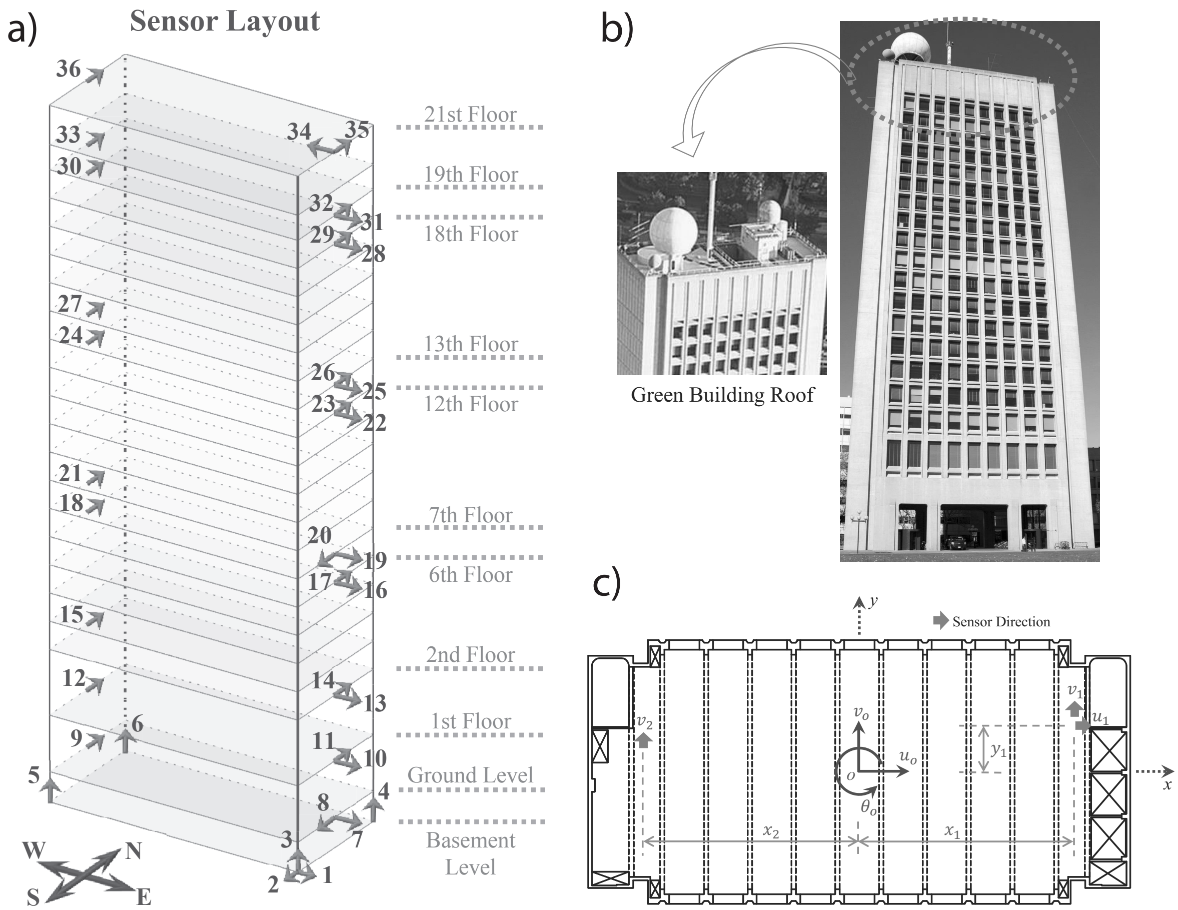

Figure 1: Sensor layout in the Green building. a) Location and orientation of the 36 accelerometers within the Green building. b) Picture of the southern side of the Green building with the structures on the roof. c) A map view of a typical floor of the Green building with the location of the three accelerometers in the $x - O - y$ coordinate system. Note the elevator shafts on the eastern side of the building.

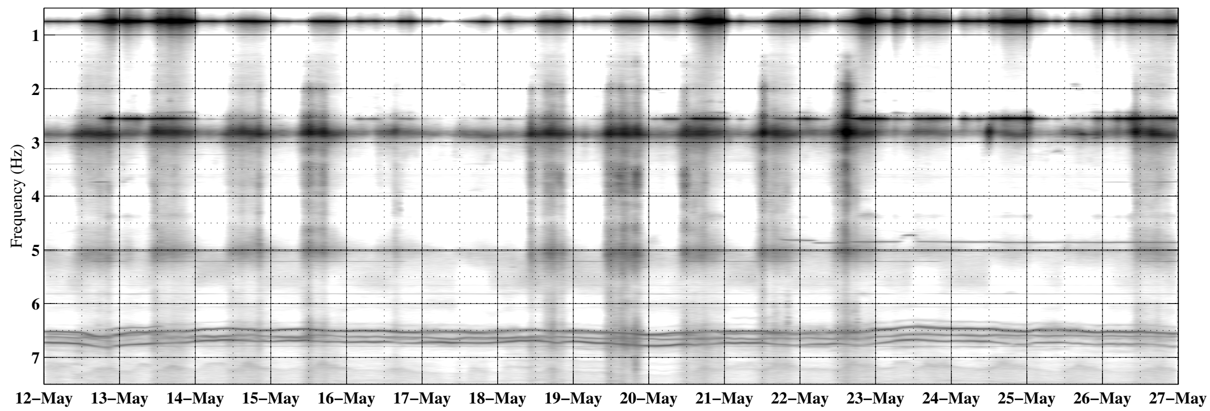

Figure 2: Spectrogram of the NS acceleration v_0 recorded on the roof of the Green building during the two weeks experiment. Plain vertical lines correspond to midnight, dotted vertical lines correspond to midday.

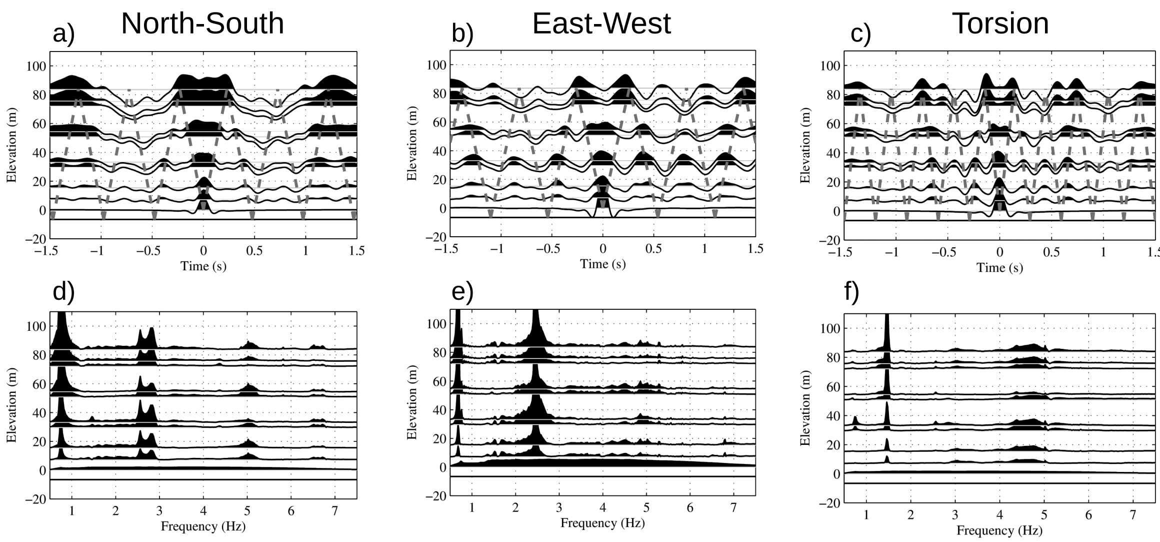

Figure 3: Estimated Impulse Response Functions (IRFs) of the Green building, filtered between 0.5 and 7.5 Hz. a) Waveforms of the NS translational modes at each floor from a source at the ground level. b) same as a) for the EW translational modes. c) same as a), for the torsional modes. The gray dashed lines in frames a), b) and c) show the travel time of the shear-wave traveling up and down inside the building at the constant speed of ∼365 m/s, ∼320 m/s and ∼600 m/s for the NS translational modes, EW translational modes and torsional modes, respectively. Note that the waves reflect at the basement level with a negative reflection coefficient. Frames d), e) and f) show the power spectra of the waveforms shown in frame a), b) and c), respectively.

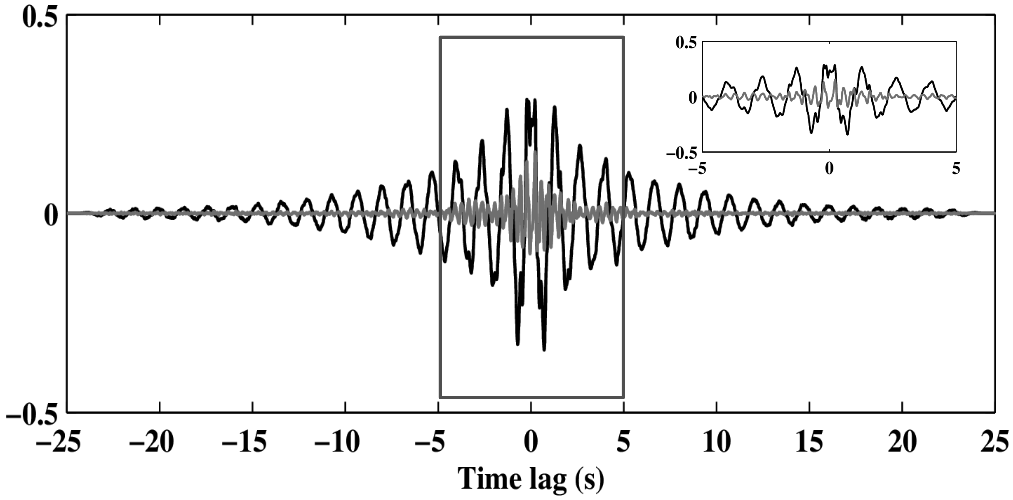

Figure 4: Estimated NS translational IRF of the Green building between the ground level and the roof, with the source at ground level, filtered between 0.5 and 7.5 Hz (black) and between 1.5 and 7.5 Hz (gray) to remove the fundamental mode. The inset is a zoom on the central part of the IRF. Note that at large time lags, high frequencies are attenuated and only fundamental mode energy remains.

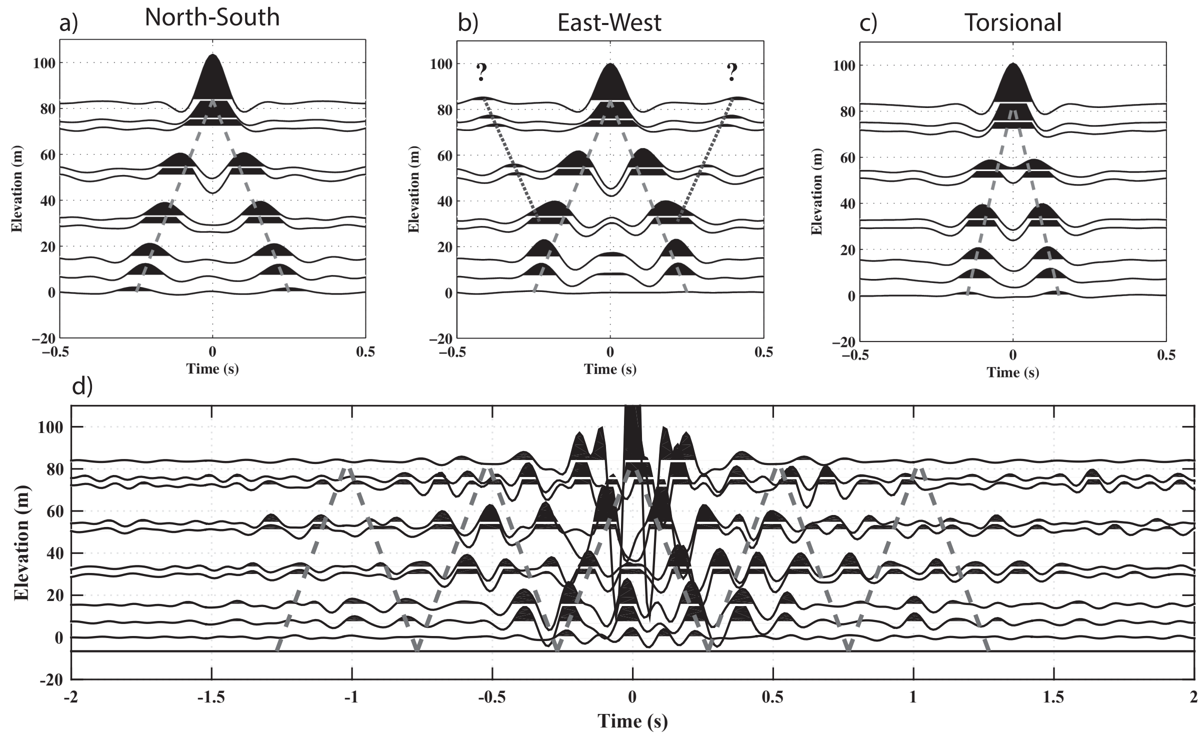

Figure 5: Estimated Impulse Response Functions (IRFs) of the Green building, filtered between 0.5 and 7.5 Hz. a) Waveforms of the NS translational modes at each floor from a source on the roof. b) same as a) for the EW translational modes. The dark-gray dotted lines highlight a phase which could be a reflection around the 3rd floor. c) same as a), for the torsional modes. The light-gray dashed lines show the travel time of the shear-wave traveling up and down inside the building at the constant speed of $\sim$335 m/s, $\sim$320 m/s and $\sim$600 m/s for the NS translational modes, EW translational modes and torsional modes, respectively. d) Waveforms of the NS translational modes at each floor from a source on the roof, filtered between 4 and 10 Hz to highlight the coda of the waveforms. The coda is partly made of reflections at the base of the building (the dashed lines are illustrative reflections with $\sim$335 m/s wave speed).

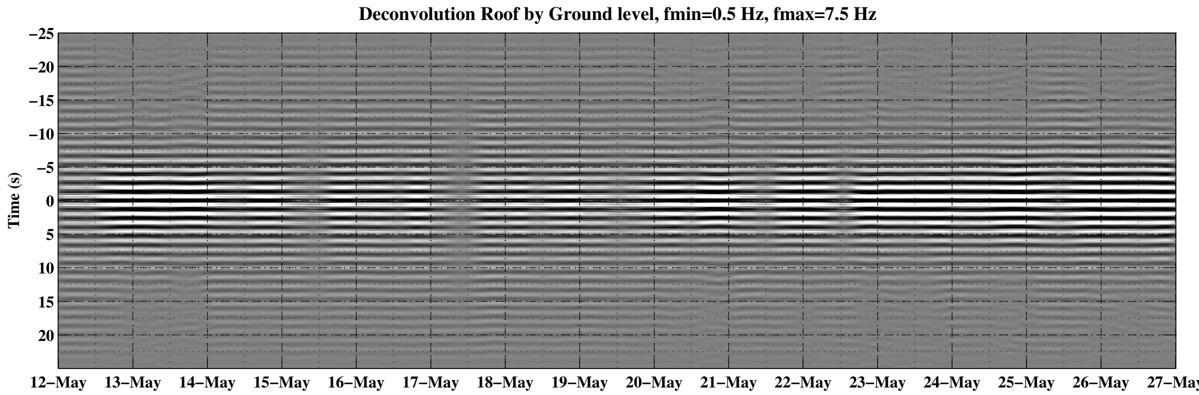

Figure 6: Estimated IRFs of the Green building for the NS translational modes, filtered between 0.5 and 7.5 Hz. The vertical dashed lines indicate midnight and the vertical dotted lines indicates midday.

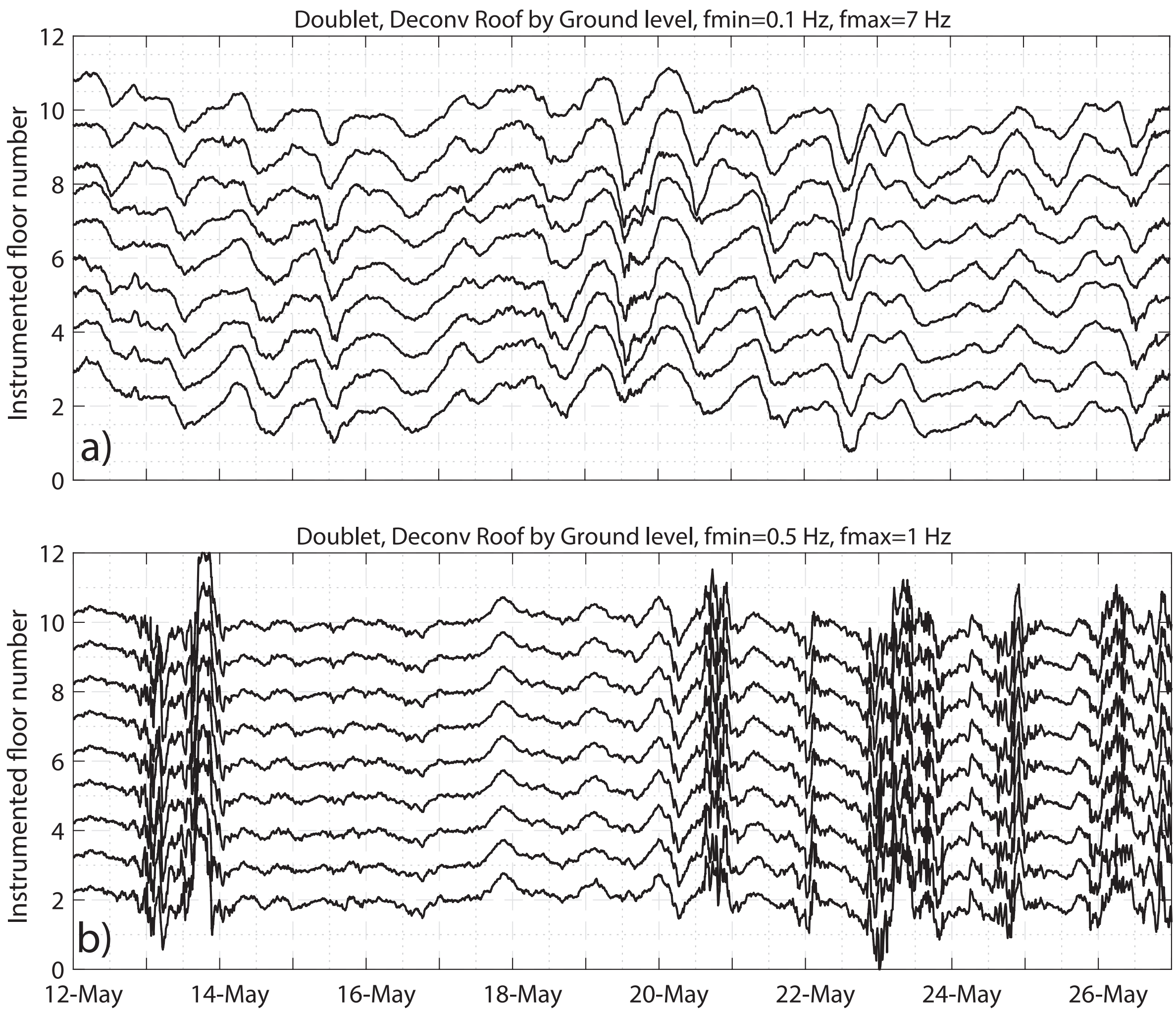

Figure 7: Velocity variations (dv/v) measured on the NS translational modes IRFs. a) dv/v at each instrumented floor measured in the central part of the IRFs (-3 s $< t <$ 3 s) with the MWCS method, between 0.1 and 7.0 Hz. b) Same as a) but measured on the later part of the IRFs (15 s $< |t| <$ 24.5 s), between 0.5 and 1.0 Hz.

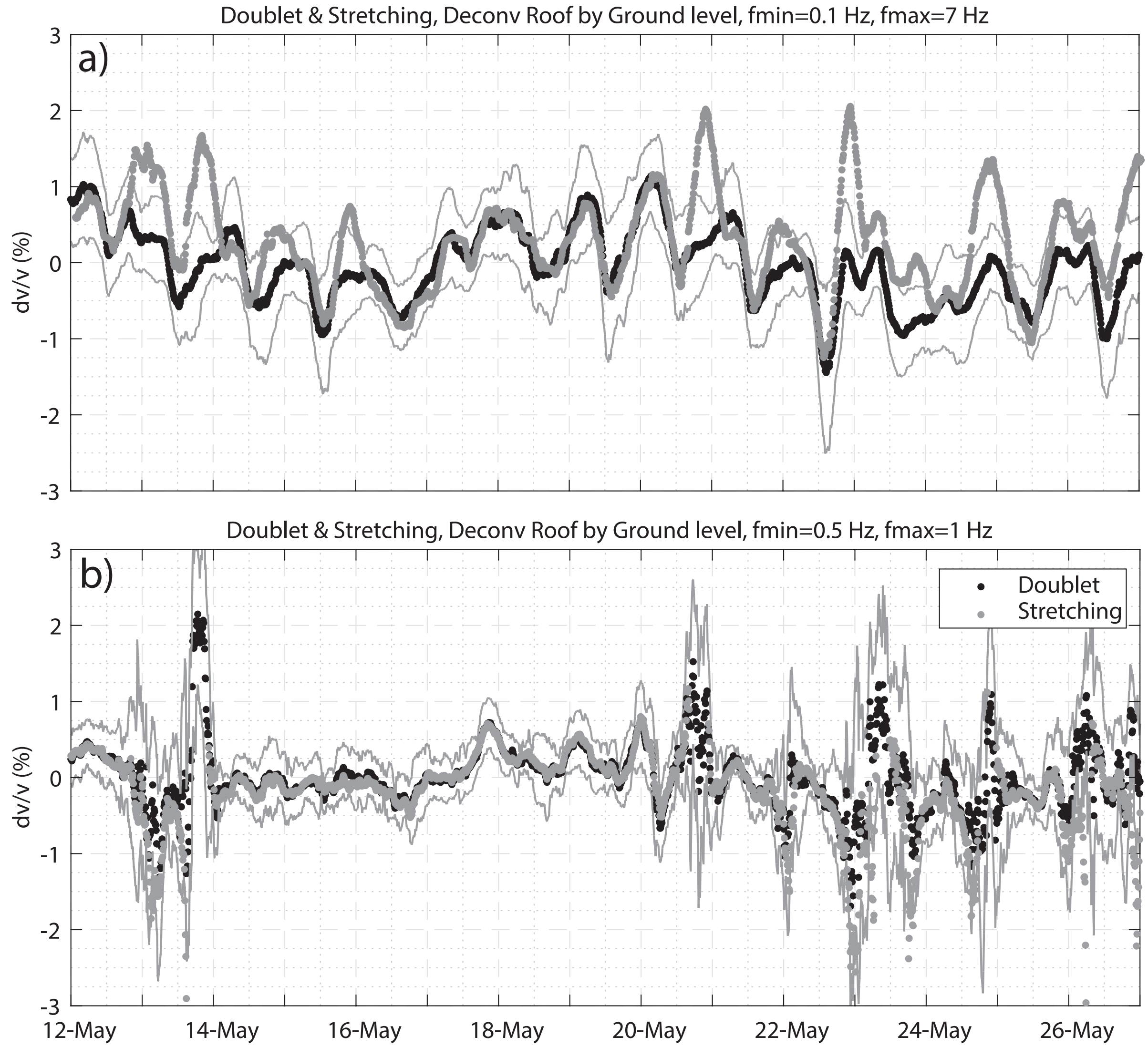

Figure 8: a) Comparison of dv/v measured on the roof within the central part of the IRFs (-3 s $< t <$ 3 s) using MWCS (black dots) and ST (gray dots), between 0.1 and 7.0 Hz. b) Same as a) but measured on the later part of the IRFs (15 s $< |t| <$ 24.5 s), between 0.5 and 1.0 Hz to focus only on the fundamental mode. The gray lines show the measurements uncertainties (here centered on the MWCS measurements).

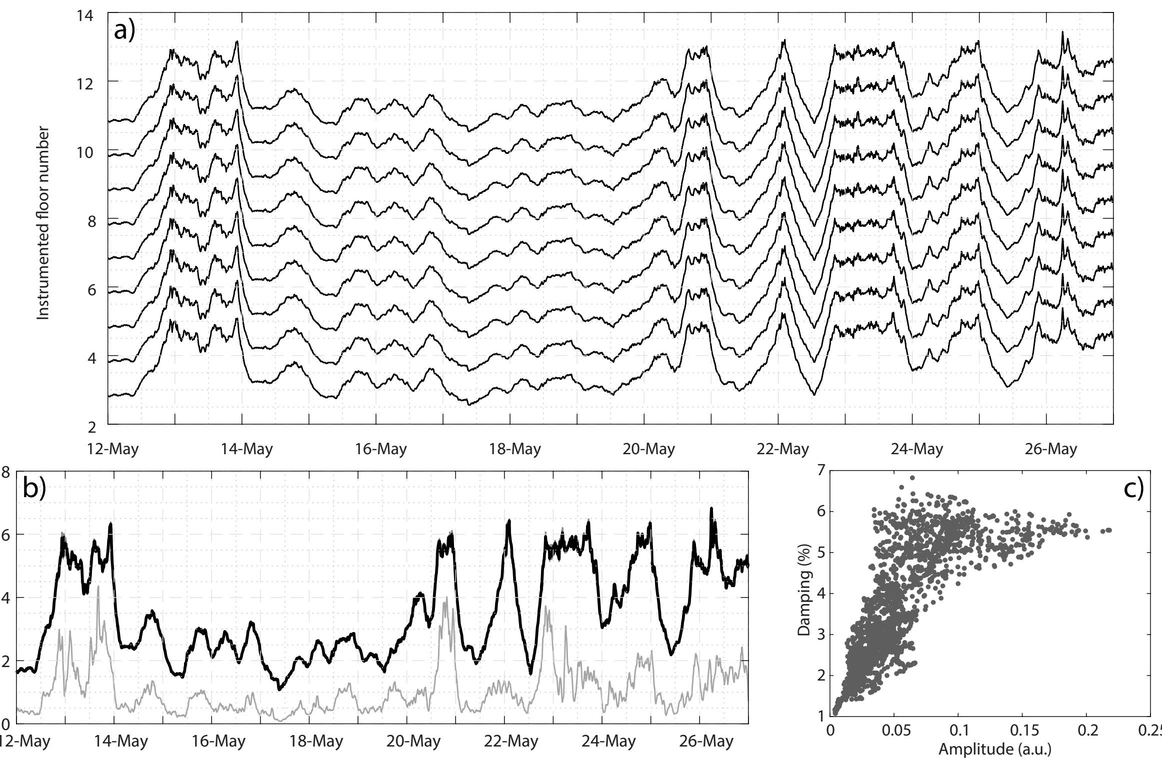

Figure 9: Apparent damping variations measured for the NS fundamental translational mode with virtual source at the ground floor. a) Apparent damping variations at each instrumented floor. b) Apparent damping variations averaged over all floors. The standard deviation is on the order of the thickness of the line and is not visible. The thin gray curve shows the amplitude of the NS fundamental translational mode recorded on the roof. c) Correlation between the amplitude of the NS fundamental translational mode and the apparent damping.

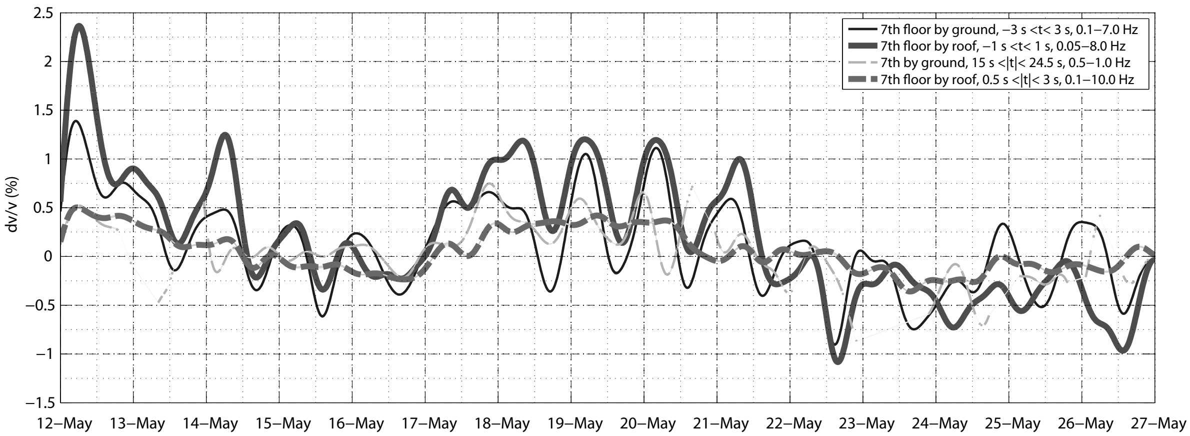

Figure 10: Velocity variations (dv/v) measured on the NS translational modes IRFs for different windows along the waveforms (plain curves for the central parts, dashed curves for the coda parts) and different virtual sources: either the 7th floor deconvolved by the ground floor (thin curves) or the 7th floor deconvolved by the roof (thick curves).

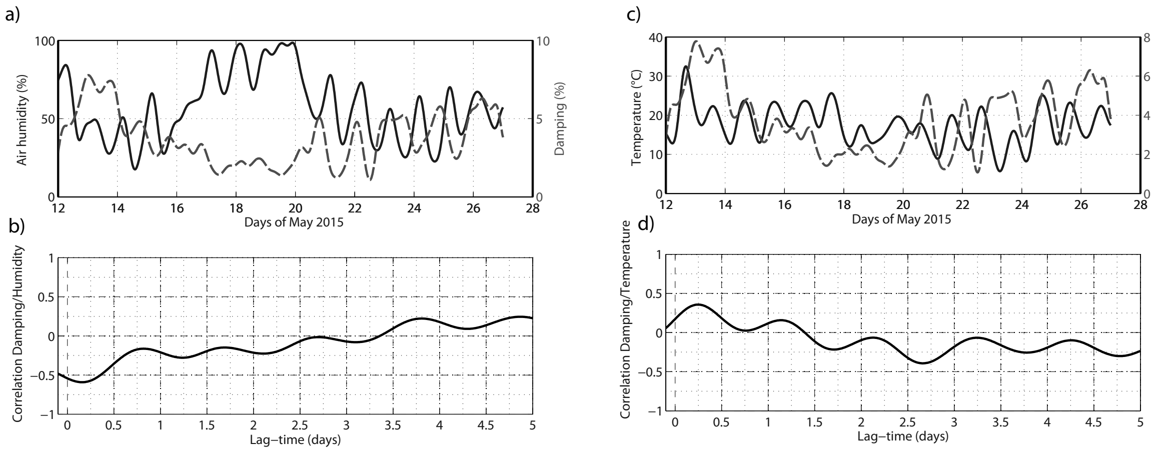

Figure 11: Comparison between the measured amplitude decay (damping) of the NS fundamental translational mode and two weather parameters. a) Damping (dashed line) vs. air humidity filtered between 6 and 400 hours of period. b) The cross-correlation between the two curves shown in a). Only the positive time-lag is shown to focus on causality between the weather forcing and the observed damping. c) Damping (dashed line) vs. temperature filtered between 6 and 400 hours of period. d) The cross-correlation between the two curves shown in c).

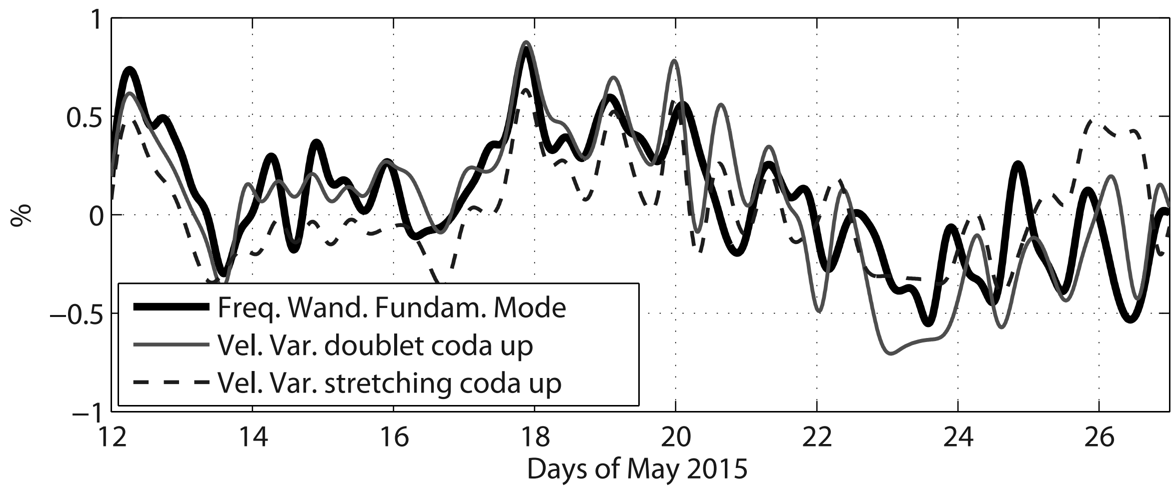

Figure 12: Comparison of the frequency wandering of the NS fundamental mode (~ 0.75 Hz) with velocity variations of the NS translational modes IRFs measured on the later part of the up-going IRFs, filtered between 0.5 and 1.0 Hz using the MWCS and stretching methods. Both dv/v and frequency wandering curves (expressed in %) are filtered between 6 and 400 hours of period.

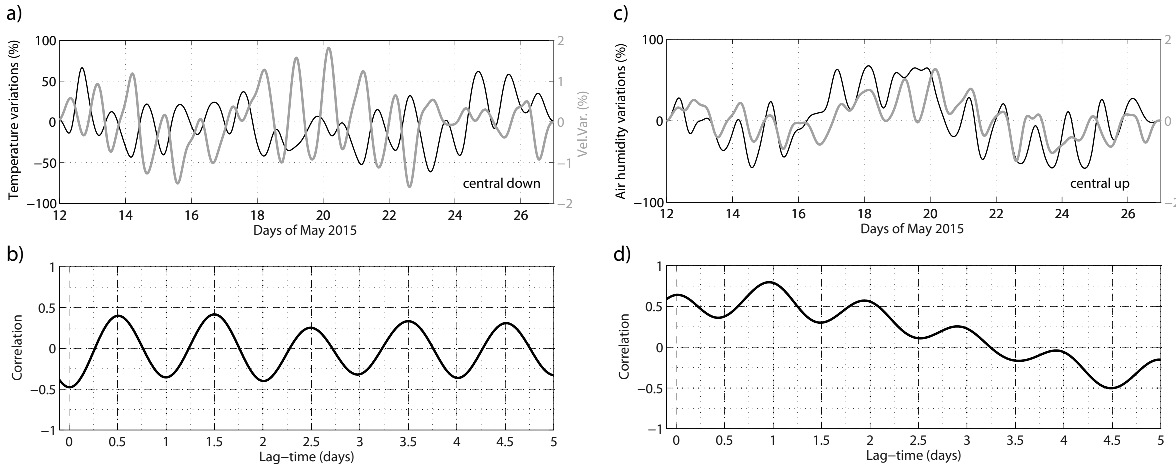

Figure 13: Comparison and cross-correlation between weather parameters and relative velocity variations. a) Relative change in temperature vs. relative velocity variations measured on the central part of the down-going IRFs. b) Causal part of the cross-correlation between the two curves presented in a). c) Relative change in humidity vs. relative velocity variations measured on the central part of the up-going IRFs. d) Causal part of the cross-correlation between the two curves presented in c).

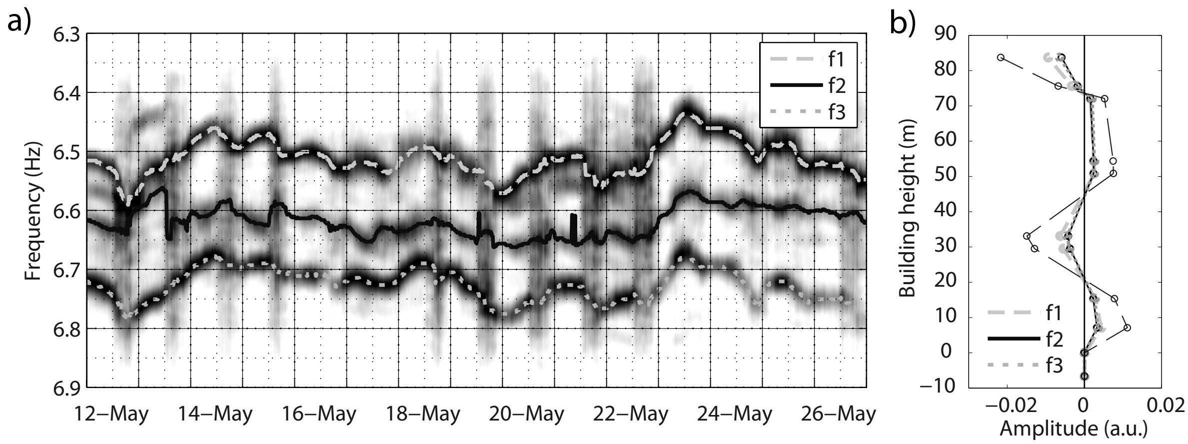

Figure 14: The 4th NS translational mode (3rd overtone). a) Automatic picking of the three singlets of the NS 4th translational mode on top of a zoomed section of the spectrogram presented in Fig. 2. b) Mode shapes computed from the up-going IRFs averaged over May 17 and filtered around each individual singlet (light gray dashed line for f_1, plain black line for f_2 and gray dotted line for f_3) and for the three singlets taken altogether (dark gray long-dashed line).

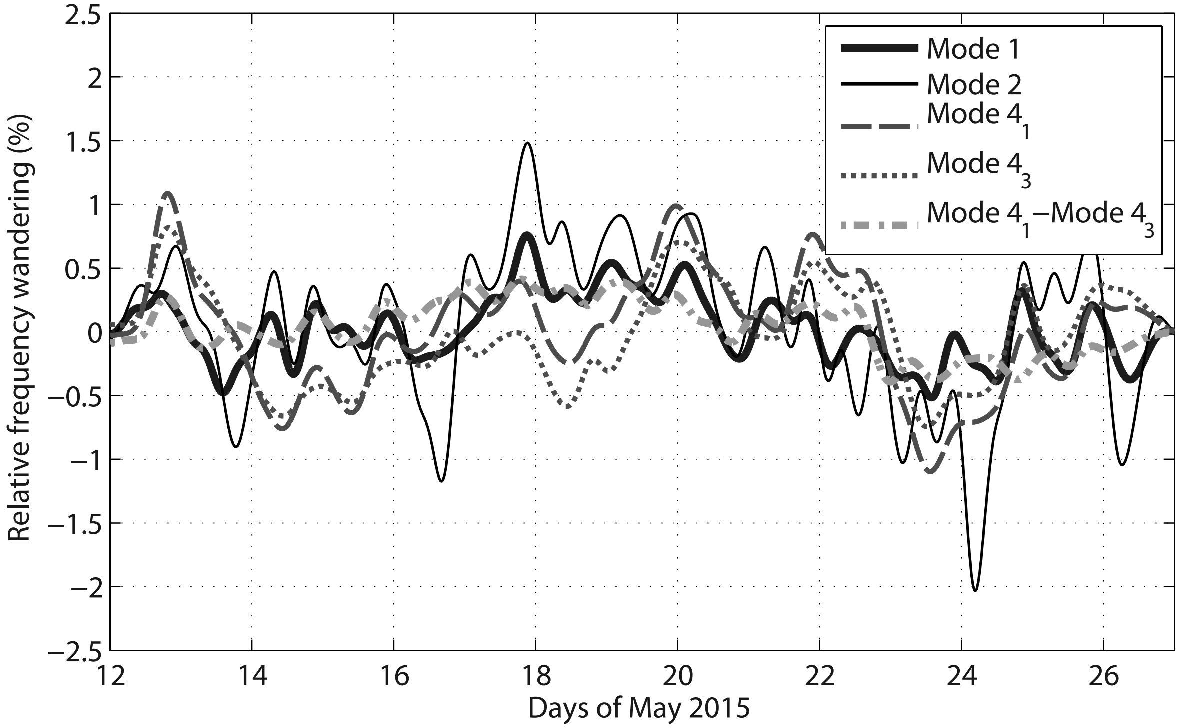

Figure 15: Relative frequency wandering of the first, second and fourth NS translational modes and wandering of the difference between the two strongest singlets of the fourth mode.

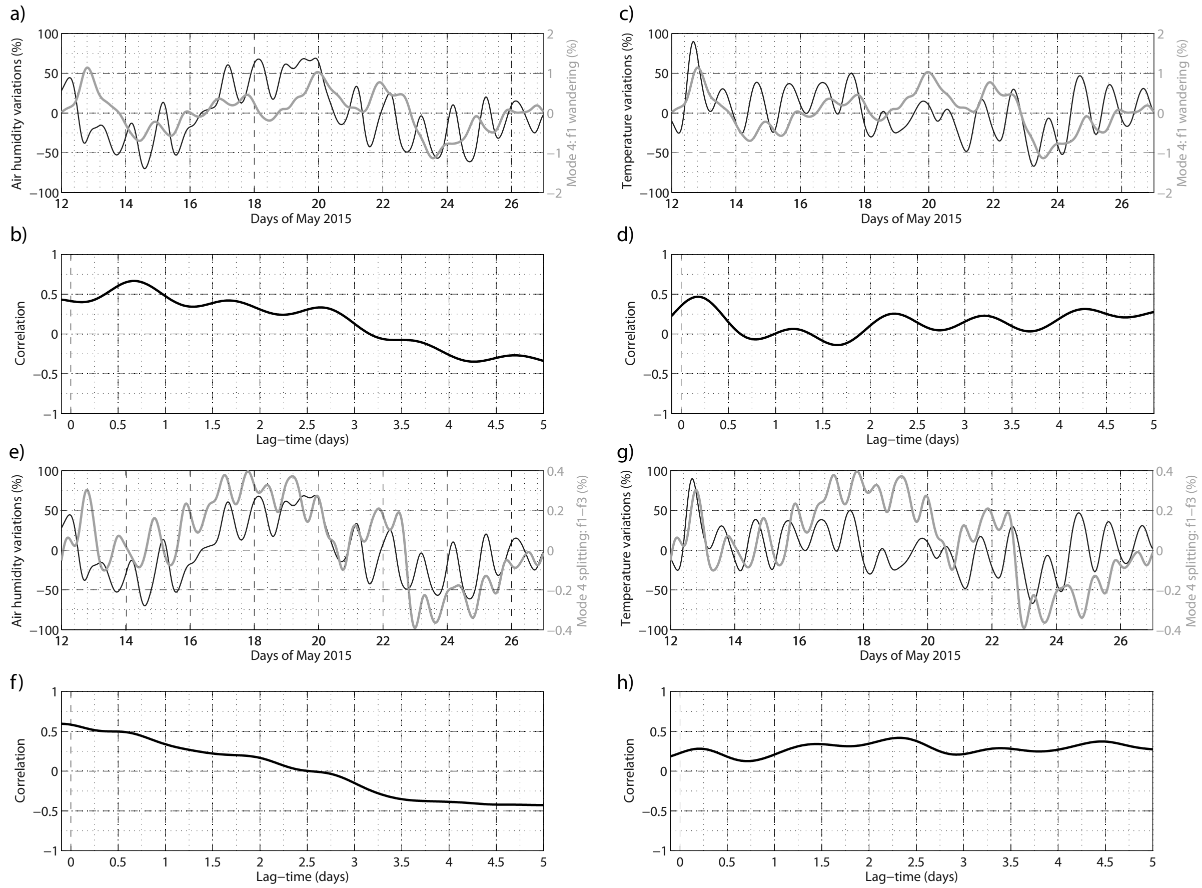

Figure 16: Correlation analysis of the NS 4th mode (see Figure 14 for the definition of f_1 and f_3) vs. weather parameters variation measured on top of the Green building. Both $f_3 - f_1$ and weather parameters curves (expressed in %) are filtered between 6 and 400 hours of period prior to the correlation analysis. a) Comparison between the temperature and the first singlet f_1 of the 4th NS translational mode. b) Cross-correlation between the two curves shown in a). c) and d) Same as a) and b) for the humidity. e) Comparison between the temperature and the difference between the first (f_1) and third (f_3) singlets of the 4th NS translational mode. f) Cross-correlation between the two curves shown in e). g) and h) Same as e) and f) for the humidity.